



Proceedings of the Eleventh International Conference on
Engineering Computational Technology
Edited by B.H.V. Topping and P. Iványi
Civil-Comp Conferences, Volume 2, Paper 5.2
Civil-Comp Press, Edinburgh, United Kingdom, 2022, doi: 10.4203/ccc.2.5.2
©Civil-Comp Ltd, Edinburgh, UK, 2022

Bending and Buckling of Shear-elastic Angle-ply Laminated Plates using Enhanced Refined Zigzag Theory

H. Wimmer^{1,2}, Ch. Celigoj³, R. Timmers⁴

¹**Civil Engineering Department, University of Applied Sciences
Upper Austria, Wels, Austria**

²**Civil Engineering Department, Carinthia University of Applied
Sciences, Spittal/Drau, Austria**

³**Institute of Strength of Materials
Graz University of Technology, Graz, Austria**

⁴**Unit of Steel Construction and Mixed Building Technology
University of Innsbruck, Innsbruck, Austria**

Abstract

Multi-layered composite and sandwich plates are increasingly being used in structures of aerospace, marine, civil and automotive areas. Each can exhibit anisotropic behaviour and drastically varying transverse shear flexibility. Such highly heterogeneous cross-sections show a significant deviation from the kinematic hypothesis that is usually applied in classical plate theories. With the recently presented enhanced Refined Zigzag Theory (en-RZT) it is possible to model the specific warping effects that occur in shear-elastic cross-ply or angle-ply laminates. By expanding the kinematic equations with to so-called von Karman terms the geometric stiffness matrix is derived, and linear buckling applications are verified. The triangular, C^0 -continuous element, originally introduced by Tessler and extended by Versino, has seven degrees of freedom per node. It shows good convergence and accuracy in thick and thin configurations.

Keywords: refined zigzag theory, angle-ply multi-layered plates, buckling.

1 Introduction

Multi-layered composite and sandwich plates are increasingly being used in structures of aerospace, marine, civil and automotive areas. Since each individual layer is to perform a specific function, different materials are used, most of which can exhibit anisotropic behaviour and drastically varying transverse shear flexibility. Such highly heterogeneous cross-sections show a significant deviation from the kinematic hypothesis that is usually applied in classical plate theories such as that of Kirchhoff or Reissner/Mindlin [1]. To model cross-sectional distortions higher-order single-layer theories or layer-wise theories have been devised. The former does not always deliver sufficiently good results, while the latter involves a great deal of numerical effort. A good compromise between accuracy and effort is provided by so-called zigzag theories [2]. One of them, the so-called Refined Zigzag Theory (RZT) published by Tessler/Di Sciuva/Gherlone [3] is a very robust and efficient model that uses the five global kinematic variables of the FSDT supplemented by two local variables (zigzag rotations) which control the layer-wise linear zigzag functions for the in-plane deformations. Recently Sorrenti/Di Sciuva [4] generalised the kinematics by two local warping functions (coupling terms), to predict the specific deformation phenomena that occur when dealing with angle-ply multi-layered composite plates. This newly developed model is named enhanced RZT (en-RZT). In this paper, the kinematic equations are expanded with the so-called von Karman terms leading to a geometrically non-linear version. From here the linear buckling equation can be extracted when neglecting the initial deformations.

In the present approach a triangular finite element, presented by Versino [5] is used, which employs linear shape functions for all seven nodal degrees of freedom, except for the transverse deflection where an anisoparametric interpolation is used to prevent shear locking. The implemented element shows good convergence and accuracy in thick and thin configurations.

2 Methods

We consider a laminated composite plate, embedded in three-dimensional space spanned by the global orthogonal Cartesian coordinate system $x_i (i = 1, 2, 3)$. The plate has a constant thickness h in the local direction $x_3 = z$, its mid-plane coincides with the plane $\mathbf{x}_\alpha (\alpha = 1, 2)$, as seen in Figure 1.

$$\begin{aligned} u_1^{(k)}(\mathbf{x}_\alpha, z) &= u(\mathbf{x}_\alpha) + z \cdot \theta_1(\mathbf{x}_\alpha) + \phi_{11}^{(k)}(z) \cdot \psi_1(\mathbf{x}_\alpha) + \phi_{12}^{(k)}(z) \cdot \psi_2(\mathbf{x}_\alpha) \\ u_2^{(k)}(\mathbf{x}_\alpha, z) &= v(\mathbf{x}_\alpha) + z \cdot \theta_2(\mathbf{x}_\alpha) + \phi_{21}^{(k)}(z) \cdot \psi_1(\mathbf{x}_\alpha) + \phi_{22}^{(k)}(z) \cdot \psi_2(\mathbf{x}_\alpha) \\ u_3^{(k)}(\mathbf{x}_\alpha, z) &= w(\mathbf{x}_\alpha) \end{aligned} \quad (1)$$

In Eq. (1) u, v, w are the global in-plane and out-of-plane displacements of the reference plane, $\theta_\beta(\mathbf{x}_\alpha), (\alpha, \beta = 1, 2)$ denote the global rotations about the coordinate directions \mathbf{x}_α of the reference plane and $\psi_\beta(\mathbf{x}_\alpha)$ represent the local zigzag rotations, which control the zigzag-pattern in the cross section. The mentioned

quantities form the seven kinematic degrees of freedom of the mechanical model. The four zigzag functions $\phi_{\alpha\beta}^{(k)}(z)$ are layer-wise linear functions, zero-valued at the top and the bottom of the plate, and only dependent on the layer structure, in particular on the layer thicknesses and the transverse shear moduli of the individual layers. For details on establishing these functions, please refer to [3], [4].

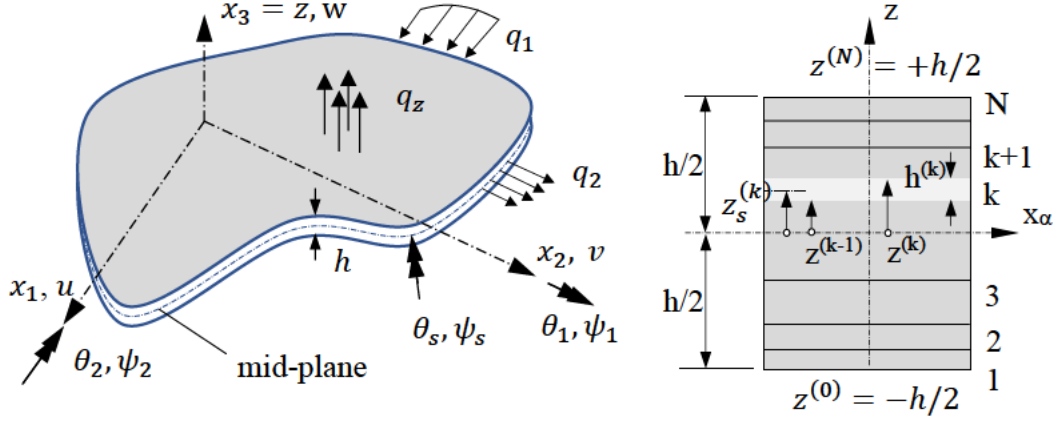


Figure 1: General plate and layer notation

Using Green-Lagrange strain-displacement relations with limitations to moderate rotations (von Karman terms), we obtain the in-plane strains

$$\mathbf{E}_p^{(k)} = \mathbf{E}^{(m)} + z \cdot \mathbf{E}^{(b)} + \mathbf{\Phi}_p^{(k)}(z) \mathbf{E}^{(\phi)} \quad (2)$$

split into the membrane part, the bending part, and the zigzag part. With the abbreviation $(\cdot)_{,\alpha} = \frac{\partial}{\partial x_\alpha}$, it follows

$$\mathbf{E}^{(m)} = \begin{pmatrix} u_{,1} + \frac{1}{2} w_{,1} \cdot w_{,1} \\ v_{,2} + \frac{1}{2} w_{,2} \cdot w_{,2} \\ u_{,2} + v_{,1} + w_{,1} \cdot w_{,2} \end{pmatrix} \quad (3a)$$

$$\mathbf{E}^{(b)} = \begin{pmatrix} \theta_{1,1} \\ \theta_{2,2} \\ \theta_{1,2} + \theta_{2,1} \end{pmatrix}, \quad \mathbf{E}^{(\phi)} = \begin{pmatrix} \psi_{1,1} \\ \psi_{2,2} \\ \psi_{1,2} \\ \psi_{2,1} \end{pmatrix} \quad (3b, c)$$

$$\mathbf{\Phi}_p^{(k)}(z) = \begin{bmatrix} \phi_{11}^{(k)} & 0 & 0 & \phi_{12}^{(k)} \\ 0 & \phi_{22}^{(k)} & \phi_{21}^{(k)} & 0 \\ \phi_{21}^{(k)} & \phi_{12}^{(k)} & \phi_{11}^{(k)} & \phi_{22}^{(k)} \end{bmatrix} \quad (4)$$

The transverse shear strains

$$\mathbf{E}_t^{(k)} = \mathbf{E}_t^{(0)} + \mathbf{\Phi}_{t,z}^{(k)}(z)\boldsymbol{\psi} = \mathbf{E}_t^{(0)} + \boldsymbol{\beta}^{(k)}\boldsymbol{\psi} \quad (5)$$

split into a constant averaged shear part and layer-dependent part give

$$\mathbf{E}_t^{(0)} = \boldsymbol{\gamma}_t^{(0)} = \begin{Bmatrix} \gamma_1^{(0)} \\ \gamma_2^{(0)} \end{Bmatrix} = \begin{Bmatrix} w_{,1} + \theta_1 \\ w_{,2} + \theta_2 \end{Bmatrix}, \quad \boldsymbol{\psi} = \begin{Bmatrix} \psi_1 \\ \psi_2 \end{Bmatrix} \quad (6a, b)$$

$$\mathbf{\Phi}_t^{(k)} = \begin{bmatrix} \phi_{11}^{(k)} & \phi_{12}^{(k)} \\ \phi_{21}^{(k)} & \phi_{22}^{(k)} \end{bmatrix} \quad (7)$$

$$\boldsymbol{\beta}^{(k)} = \frac{\partial}{\partial z} \mathbf{\Phi}_t^{(k)} = \begin{bmatrix} \beta_{11}^{(k)} & \beta_{12}^{(k)} \\ \beta_{21}^{(k)} & \beta_{22}^{(k)} \end{bmatrix} \quad (8)$$

According to the assumption of plane stress state ($S_{33} = 0$), these strains are connected by the elastic Hookean law with the corresponding second Piola-Kirchhoff stress quantities.

$$\mathbf{S}_p^{(k)} = \begin{Bmatrix} S_{11} \\ S_{22} \\ S_{12} \end{Bmatrix}^{(k)} = \bar{\mathbf{Q}}_p \mathbf{E}_p^{(k)}, \quad \mathbf{S}_t^{(k)} = \begin{Bmatrix} S_{13} \\ S_{23} \end{Bmatrix}^{(k)} = \bar{\mathbf{Q}}_t \mathbf{E}_t^{(k)} \quad (9a, b)$$

The matrices $\bar{\mathbf{Q}}$ contain the transformed plane stress-reduced stiffness coefficients [1].

$$\bar{\mathbf{Q}}_p^{(k)} = \begin{bmatrix} \bar{Q}_{11} & \bar{Q}_{12} & \bar{Q}_{16} \\ \bar{Q}_{12} & \bar{Q}_{22} & \bar{Q}_{26} \\ \bar{Q}_{16} & \bar{Q}_{26} & \bar{Q}_{66} \end{bmatrix}^{(k)}, \quad \bar{\mathbf{Q}}_t^{(k)} = \begin{bmatrix} \bar{Q}_{44} & \bar{Q}_{45} \\ \bar{Q}_{45} & \bar{Q}_{55} \end{bmatrix}^{(k)} \quad (10a, b)$$

To establish the discretized problem the principle of virtual work says

$$\delta W_{int} - \delta W_{ext} = 0 \quad (11)$$

In detail, it reads

$$\delta W_{int} = \int \delta \mathbf{E}_p^T \mathbf{S}_p dV + \int \delta \mathbf{E}_t^T \mathbf{S}_t dV \quad (12)$$

Integration over the thickness of the first part leads to

$$\delta W_{int} = \int \delta \mathbf{E}_p^T \mathbf{R}_p dA + \int \delta \mathbf{E}_t^T \mathbf{R}_t dA \quad (13)$$

with the second Piola-Kirchhoff-stress resultants

$$\mathbf{R}_p = \begin{Bmatrix} \mathbf{N} \\ \mathbf{M} \\ \mathbf{M}_\phi \end{Bmatrix}, \quad \mathbf{R}_t = \begin{Bmatrix} \mathbf{T} \\ \mathbf{T}_\phi \end{Bmatrix} \quad (14)$$

Their components are defined by

$$(\mathbf{N}, \mathbf{M}, \mathbf{M}^{(\phi)}) = \left(\begin{array}{c} \begin{Bmatrix} N_{11} \\ N_{22} \\ N_{12} \end{Bmatrix}, \begin{Bmatrix} M_{11} \\ M_{22} \\ M_{12} \end{Bmatrix}, \begin{Bmatrix} M_{11}^{(\phi)} \\ M_{22}^{(\phi)} \\ M_{12}^{(\phi)} \\ M_{21}^{(\phi)} \end{Bmatrix} \end{array} \right) = \int_{-\frac{h}{2}}^{+\frac{h}{2}} (1, z, \boldsymbol{\Phi}_p^{(k)T}(z)) \mathbf{S}_p^{(k)} dz \quad (15a)$$

$$(\mathbf{T}, \mathbf{T}^{(\phi)}) = \left(\begin{array}{c} \begin{Bmatrix} T_1 \\ T_2 \end{Bmatrix}, \begin{Bmatrix} T_1^{(\phi)} \\ T_2^{(\phi)} \end{Bmatrix} \end{array} \right) = \int_{-\frac{h}{2}}^{+\frac{h}{2}} (1, \boldsymbol{\beta}^{(k)}) \mathbf{S}_t^{(k)} dz \quad (15b)$$

For the FE discretization, we define \mathbf{f}_{int} and \mathbf{f}_{ext} as the nodal vectors of the internal and external forces. Starting from the static equilibrium equation

$$\mathbf{f}_{int} - \mathbf{f}_{ext} = \mathbf{0} \quad (16)$$

the tangent stiffness matrix is obtained by

$$\begin{aligned} \mathbf{K}_T &= \frac{\partial \mathbf{f}_{int}}{\partial \mathbf{u}^{(e)}} = \frac{\partial}{\partial \mathbf{u}^{(e)}} \int_V \mathbf{B}^T \mathbf{S} dV = \int_V \mathbf{B}^T \frac{\partial \mathbf{S}}{\partial \mathbf{E}} \frac{\partial \mathbf{E}}{\partial \mathbf{u}^{(e)}} dV + \int_V \frac{\partial \mathbf{B}^T}{\partial \mathbf{u}^{(e)}} \mathbf{S} dV = \\ &= \int_V \mathbf{B}^T \mathbf{C} \mathbf{B} dV + \mathbf{K}_G \end{aligned} \quad (17)$$

where $\mathbf{u}^{(e)T} = [u, v, w, \theta_1, \theta_2, \psi_1, \psi_2]_i$, ($i = 1, 2, 3$) stands for the element displacement vector. The stability problem then appears as a linear eigenvalue problem with \mathbf{K}_L as the linear stiffness matrix and the eigenvalue λ as a load-increasing factor concerning the initial stress state to produce the bifurcation limit of static equilibrium.

$$(\mathbf{K}_L + \lambda \mathbf{K}_G) \mathbf{u} = \mathbf{0} \quad (18)$$

For details concerning the shape functions and the matrices see [5-8].

3 Results

As a first example the bending-stretching coupling effect of a two-layered thin strip in tension is investigated. The thin strip has a ratio $a_1/a_2 = 400/100$ mm and two layers with thickness $t_1 = 1.6$ mm each, in angle-ply ($\pm 45^\circ$) configuration. The strip is loaded by uniaxial tension $q_1 = 100$ N/mm. The material data are as follows: $E_1 = 31100$ N/mm², $E_2 = E_3 = 7600$ N/mm², $G_{12} = G_{13} = 2900$ N/mm², $G_{23} = 2600$ N/mm², $\nu_{12} = \nu_{13} = 0.303$, $\nu_{23} = 0.462$. The left and right edge, where the line loads are acting in opposite directions, is fixed ($v = w = 0$).

The midpoint of the strip is constrained for kinematic determinacy ($u = 0$). Figure 2 shows the deflection w of the strip.

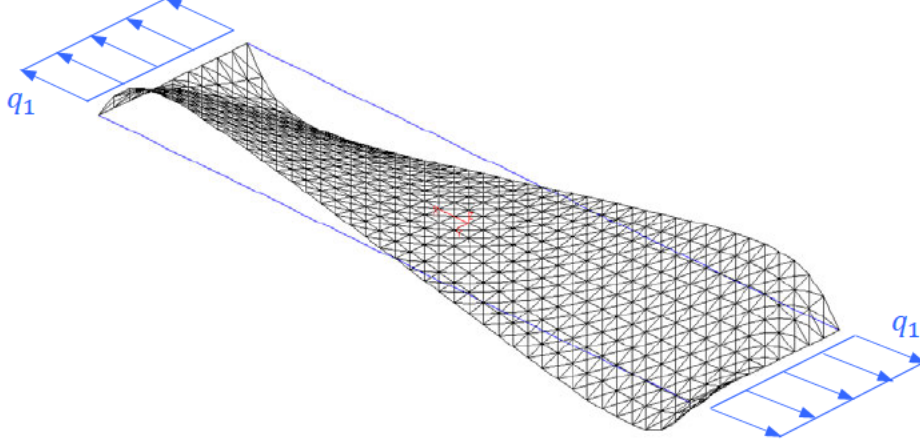


Figure 2: Skew symmetric deformation of a thin two-layer angle-ply strip under uniaxial tension (mesh pattern 40x10).

	Max. $ u $ [mm]	Max. $ v $ [mm]	Max. $ w $ [mm]
en RZT	0.686	0.104	0.128
ANSYS-3D (SOLID186)	0.686	0.104	0.102
ANSYS-3D (SOLID185)	0.686	0.104	0.121

Table 1: Maximum displacements (linear analysis) of a thin strip under uniaxial tension.

For comparison, the strip is analysed by a high-resolution 3D model [9] (see Table 1). Therefore, the element type SOLID186 with 20 nodes is chosen. Using SOLID185 with 8 nodes and only one element layer for each material layer the warping is forced to be linear, and the deflection coincides with the plate solution.

A second example, the bending of a simply supported quadratic plate is considered in a linear analysis. The plate has two layers of equal thickness (fibre orientation $\pm\theta^\circ$, plate centre at $x_1/x_2 = \frac{a_1/a_2}{2}$). The span-thickness ratio is $a_1/h = 10$. Material data: $E_1 = 25 \text{ MN/m}^2$, $E_2 = E_3 = 1.0 \text{ MN/m}^2$, $G_{12} = G_{13} = 0.50 \text{ MN/m}^2$, $G_{23} = 0.20 \text{ MN/m}^2$, $\nu_{12} = \nu_{13} = \nu_{23} = 0.25$. The plate is loaded by a bi-sinusoidally distributed surface load $q_z(x_1, x_2) = q_0 \sin\left(\frac{\pi x_1}{a_1}\right) \sin\left(\frac{\pi x_2}{a_2}\right)$. For comparison, we refer to an existing 3D-analytical solution given by Savoia and Reddy [10] and an analytical solution based on enhanced RZT recently presented by Sorrenti and Di Sciuva [4]. The discretisation is done for the entire plate using the mesh type shown in Figure 2.

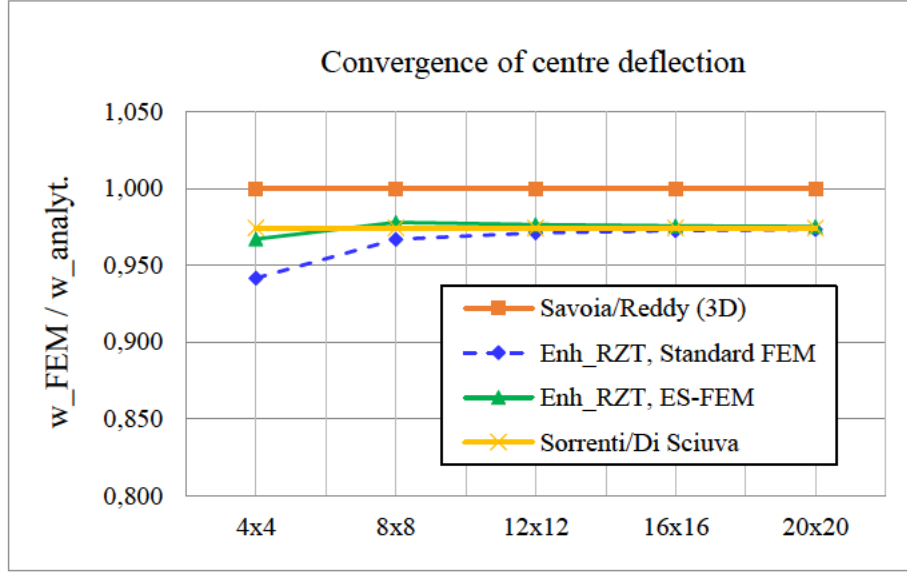


Figure 3: Convergence of centre deflection w of a square angle-ply plate ($\theta = \pm 15^\circ$)

As can be seen from Figure 3 the FE solution shows very good convergence concerning the analytical solutions. The plate solution is slightly stiffer than the 3D-solution when at the simply supported boundaries the normal rotations θ_s , ψ_s are set to zero (stiff bearing, see Figure 1). For details see [4], [10]. As in previous work, it was found in most cases that the edge-based smoothed variant (ES-FEM) [7] leads to a better convergence rate.

In a last example, the buckling of a simply supported, rectangular, laminated plate with four layers of the same thickness and with fibre orientation $(+\theta/-\theta/+\theta/-\theta)$ is considered. The plate has a length in direction x_1 of $a_1 = 1.00$ m and is loaded by a constant uniaxial stress field in this direction. Different geometries (aspect ratio a_1/a_2), fibre directions ($\pm \theta^\circ$) and span-to-thickness ratios (a_1/h) have been studied. Material data: $E_1 = 40$ MN/m², $E_2 = E_3 = 1.0$ MN/m², $G_{12} = G_{13} = 0.60$ MN/m², $G_{23} = 0.50$ MN/m², $\nu_{12} = \nu_{13} = \nu_{23} = 0.25$. We applied two different types of boundary conditions:

Case A (in accordance to SS-2 in [5], plate centre at $x_1/x_2 = 0/0$)

means @ $x_1 = \pm a_1/2$: $u = w = \theta_2 = \psi_2 = 0$ and @ $x_2 = \pm a_2/2$: $v = w = \theta_1 = \psi_1 = 0$ (stiff bearing) and

Case B

means @ $x_1 = \pm a_1/2$: $w = 0$ and @ $x_2 = \pm a_2/2$: $w = 0$ (weak bearing).

Table 2 and 3 show the results concerning $a_1/h = 50$. The results of the 3D calculations are slightly lower than the 2D calculations. This is probably due to the direct load introduction via the transverse edges. In addition, we found effects in the thickness direction, especially for the thick plate with $a_1/h = 10$, which will be examined in more detail in future investigations.

a ₁ /h	θ[°]	a ₁ /a ₂									
		0.50					1.00				
		[11]	[5]	FEM 2D (A)	FEM 2D (B)	FEM 3D (B)	[11]	[5]	FEM 2D (A)	FEM 2D (B)	FEM 3D (B)
50	30	0.938	0.944	0.947	0.930	0.904	1.939	1.959	1.965	1.871	1.771
	45	0.719	0.723	0.726	0.695	0.674	2.174	2.199	2.207	2.052	1.937
	60	0.450	0.453	0.454	0.435	0.420	1.939	1.959	1.785	1.680	1.576

Table 2: Critical buckling stress (in N/mm²) for uniaxial compressive load, simply supported on all edges and a₁/h = 50. Values above must be divided by 100.

a ₁ /h	θ[°]	a ₁ /a ₂ = 2.00				
		[11]	[5]	FEM 2D (A)	FEM 2D (B)	FEM 3D (B)
50	30	6.927	7.057	7.075	6.425	5.979
	45	10.93	11.20	8.330	7.395	6.752
	60	14.16	14.52	6.440	5.780	5.212

Table 3: Critical buckling stress (in N/mm²) for uniaxial compressive load, simply supported on all edges and a₁/h = 50. Values above must be divided by 100.

4 Conclusions and Contributions

The Refined Zigzag Theory is a powerful and reliable theory for the accurate detection of stresses and deformations of shear-elastic, cross-ply laminated plates. In the recently presented enhanced version, it can deal with angle-ply plates in which two adjacent laminae have alternating orientations, but the same absolute value. In this contribution, the performance of a simple triangular plate element is illuminated for the linear bending and buckling case of such plates. The results match well with the few values given in the literature. Certain differences make further investigations necessary.

References

- [1] J.N. Reddy, "Mechanics of Laminated Composite Plates and Shells", 2nd Edition, CRC Press, New York, 2004.
- [2] E. Carrera, "Historical review of zig-zag theories for multi-layered plates and shells", Appl. Mech. Reviews, 56(3), 287–308, 2003.
- [3] A. Tessler, M. Di Sciuva, M. Gherlone, "A consistent refinement of first-order shear deformation theory for laminated composite and sandwich plates using improved zigzag kinematics", J. Mech. Mat. Struct., 5(2), 341–367, 2010.
- [4] M. Sorrenti, M. Di Sciuva, "An Enhancement of Warping Shear Functions of Refined Zigzag Theory", J. Appl. Mech., 88, 084501-1–084501-7, 2021.

- [5] M. Sorrenti, M. Gherlone, M. Di Sciuva, “Buckling analysis of angle-ply multilayered and sandwich plates using the enhanced Refined Zigzag Theory”, *Proceedings of the Estonian Academy of Sciences*, 71(1), 84–102, 2022.
- [6] D. Versino, M. Gherlone, M. Mattone, M. Di Sciuva, A. Tessler, “ C^0 -triangular elements based on the refined zigzag theory for multi-layered composite and sandwich plates”, *Compos. Part B*, 44(1), 218–230, 2013.
- [7] H. Wimmer, Ch. Celigoj, “An edge-based smoothed three-node composite plate element with refined zigzag kinematics”, *Compos. Struct.*, 274, 114204, 2021.
- [8] H. Wimmer, Ch. Celigoj, “A new approach for buckling analysis of laminated glass panels”, *7th World Multidisciplinary Civil Engineering – Architecture – Urban Planning – Symposium (WMCAUS) 2022*, Prague.
- [9] ANSYS Engineering Simulation & 3D Design Software. Available online: <https://www.ansys.com/>
- [10] M. Savoia, J.N. Reddy, “A Variational Approach to Three-Dimensional Elasticity Solutions of Laminated Composite Plates”, *ASME J. Appl. Mech.*, 59 (2S), 166-175, 1992.
- [11] H. Matsunaga, “Vibration and Stability of angle-ply laminated composite plate subjected to in-plane stresses”, *Int. J. Mech. Sci.*, 43(8), 1025-1944, 2001.